Available online at www.sciencedirect.com
SCIENCE DIRECT
Acta Materialia 54 (2006) 953–961
Acta MATERIALIA
www.actamat-journals.com

Computer modeling and simulation of solid-state sintering: A phase field approach

Yu U. Wang *

Department of Materials Science and Engineering, Virginia Tech, 211A Holden Hall (0237), Blacksburg, VA 24061, USA

Received 6 August 2005; accepted 7 October 2005
Available online 9 December 2005

Abstract

A phase field model of solid-state sintering is developed. The model treats multiple concurrent physical processes, i.e., rigid-body translation and rotation of powder particles, grain growth through boundary migration, and various diffusion mechanisms including surface diffusion, grain boundary diffusion, volume diffusion, and vapor transport through evaporation and condensation. The approach of centers of particles through rigid-body motions plays a key role in the densification of sintered powder compacts. The effective treatment of particle translation and rotation in phase field formalism is a necessary and critical step in developing a phase field sintering model. A scheme of particle translation and rotation is formulated based on a new formula of grain boundary force. The rigid-body motion modifies both the Cahn–Hilliard nonlinear diffusion equation and the Ginzburg–Landau (Allen–Cahn) structural relaxation equation by introducing advection terms. Computer simulations are presented.

Keywords: Phase field model; Sintering; Diffusion; Grain boundary migration; Microstructure

1. Introduction

Sintering is one of the most important materials processing techniques. Modern sintering technology has tremendous importance in the powder metallurgy and ceramics industry [1]. Recently, sintering has been used to fabricate multiferroic/magnetoelectric composites [2–5]. Nanopowder sintering has become one of the primary processing routes to nanocrystalline materials [6]. Sintering is also related to other manufacturing processes, e.g., constrained-film sintering of circuit paste (nanopowder) in microelectronics packaging [7], fabrication of coatings by sintering powders onto substrates [8], etc.

Sintering is a well-known complicated material processing technique. It involves multiple simultaneous physical processes, including various diffusion paths (along surface and grain boundary, through bulk lattice), vapor transport (through evaporation and condensation), particle rigid-body motions (translation and rotation), and grain growth through boundary migration [1,9]. The sintering kinetics depends on the interactions among these processes as well as the interdependence of these processes and the evolving powder compact microstructure (shape, size, relative location, and crystallographic orientation of individual particles/grains). The collective sintering behavior results in two competing phenomena, i.e., densification and grain growth. Precise control of densification and grain growth is crucial for optimization of the sintering technique and tailoring of the microstructures and properties of sintered materials. For example, processing of nanocrystalline materials requires maximum densification and minimum grain growth, while processing of porous materials preferably requires minimum densification. Experimental research alone is insufficient to gain a complete understanding of the sintering mechanisms and the consequences of densification and grain growth on the sintered microstructures and material properties. Realistic modeling and effective simulation of sintering processes is highly desirable.

* Tel.: +1 540 231 2754; fax: +1 540 231 8919.
E-mail address: yuwang@mse.vt.edu.

1359-6454/$30.00
doi:10.1016/j.actamat.2005.10.032

A sintering model of predictive value must be able to treat the multiple concurrent processes and the realistic evolving microstructure of powder compacts. Given currently available computational resources, computer modeling and simulation of sintering must adopt a mesoscopic approach. The finite element/finite difference approach has been extensively employed to study sintering problems, which is based on a continuum theory similar to continuum mechanics (e.g., see [10] for a review of the continuum sintering theory and its applications). In this approach, the surfaces and grain boundaries are special regions where boundary conditions are imposed. Such models provide a good means to test assumptions about the driving forces and boundary conditions governing sintering processes. A shortcoming of this approach is that in the numerical implementation of such models it will become increasingly difficult to account for complicated three-dimensional (3D) powder compact microstructures and complex multiple diffusion paths that both greatly influence sintering processes. Obviously, a new numerical technique is desirable, which would naturally describe the evolving microstructures of arbitrary complexity and treat surface, grain boundary and volume diffusions, vapor transport, grain boundary migration, and particle translation and rotation without explicitly tracking the surfaces and grain boundaries or imposing boundary conditions.

In this paper, a phase field sintering model is developed, which offers the appealing features mentioned above. During the past decade the phase field approach has become one of the most powerful computational methods for simulating microstructure evolutions for a wide variety of different material processes, such as solidification, solid-state phase transformations, etc. (see [11–13] for recent reviews of the phase field approach; its application to solid-state microstructure evolutions is summarized in Table 1 of Ref. [11]). In particular, the phase field approach has been employed to simulate grain growth phenomena [14–16]. One of the main advantages of the phase field approach is that it naturally describes the evolution of arbitrary microstructures without explicitly tracking interface positions or imposing ad hoc assumptions on microstructure evolution. In contrast to this, the conventional sharp-interface-based approach to microstructure evolutions tracks the location of a priori unknown interfaces; thus, its numerical implementation becomes difficult for complex 3D microstructure evolutions. The phase field model uses several continuum field functions (the so-called phase fields) to describe the sizes, shapes, and spatial arrangement of particles of different compositions, lattice symmetries, and crystallographic orientations, i.e., the microstructure, that are formed during material processing. These field variables correspond to well-defined physical parameters, such as composition in phase separation and long-range order parameters in disorder–order transitions. The field functions assume specific values in each particle and change smoothly but rapidly across interface regions (the so-called diffuse interfaces). The sharp interface model is a particular limit of the phase field model [17]. The total free energy of a material system is a functional of the phase fields, including bulk chemical free energy, interfacial energy, as well as configuration-dependent energy in the presence of long-range interactions such as elastic strain energy and electrostatic/magnetostatic energy [18–20]. Microstructure evolution is driven by a reduction of the total system free energy through diffusion and structural relaxation, and is described by the spatial and temporal changes of the phase fields. The kinetics of microstructure evolution is governed by two types of continuum equations, namely the Cahn–Hilliard nonlinear diffusion equation [21,22] for conserved composition fields and the time-dependent Ginzburg–Landau [23] (Allen–Cahn [24]) structural relaxation equation for nonconserved structural order parameter fields (see [25,26] for reviews on their applications to dynamic phenomena and phase transitions). The feature sizes of microstructures simulated by phase field models range from nanometers to micrometers (i.e., mesoscopic length scale), and the typical time of simulated microstructure evolutions is from seconds to minutes or hours (i.e., diffusion time). All these appealing features make the phase field approach a desirable choice for simulating microstructure evolution during sintering processes.

Despite the successful application of the phase field approach to a wide variety of material processes, a realistic phase field model of sintering is yet to be developed. The obstacle hindering the phase field approach to sintering is associated with the difficulty in treating the particle rigid-body motions in an effective way consistent with phase field formalism. To date, there has been only one reported attempt to incorporate rigid-body translation into a phase field model [27,28], where, however, only planar grain boundaries at fixed spatial position have been simulated. A preliminary formula relating the effective force at a grain boundary to the vacancy over-saturation at the grain

Table 1
Simulated exponents for neck growth law under different sintering mechanisms and comparison with theoretical models

Mechanism	n (for $t^* < 20$)	n (for $t^* < 100$)	n (theoretical) [1]
Grain boundary diffusion	5.52	9.04	6
Volume diffusion	5.69	6.18	5
Surface diffusion	7.43	7.32	7 (3, 5, 6, 7, 7.5)
Vapor transport	5.25	5.77	3
All modes active	7.25	6.99	–

boundary was proposed [28], but was not further exploited to develop a working scheme for the phase field approach. It is noted that without the rigid-body motion mechanism, translational motion of new phase particles has been observed in phase field simulations of two-phase systems [29]; however, such a translation is a result of pure diffusional processes through the parent phase lattice mediated by elastic stress and, thus, is fundamentally different from the particle rigid-body motion during sintering. It is also noted that a phase field model of sintering without particle rigid-body motions is equivalent to a phase field model of two-phase grain growth [30], where one of the coexisting phases is amorphous (vapor or pore) and is characterized by a mass density field only (no long-range order parameter is needed for the amorphous phase). Therefore, the effective treatment of particle translation and rotation in the phase field formalism is a necessary and critical step in developing a phase field sintering model.

This paper reports the development of a phase field model of solid-state sintering. The theoretical formulation is first presented, followed by numerical simulations, and a discussion concludes the paper.

2. Formulation

Assume that the mass of a powder compact is conserved during sintering. The mass distribution is described by a mass density field $\rho(\mathbf{r},t)$, where $\mathbf{r}$ and t are spatial position and time, respectively. The conservation of mass is characterized by the equation of continuity in terms of the density function $\rho(\mathbf{r},t)$:

$$\frac{\partial \rho}{\partial t} + \nabla \cdot (\rho \mathbf{v}) = 0, \tag{1}$$

where ∇ is gradient operator, and $\mathbf{v}(\mathbf{r},t)$ is the velocity field describing the local instantaneous motion of mass point located at position $\mathbf{r}$ at time t. The product in parentheses describes a mass flux density, i.e., $\mathbf{j} = \rho\mathbf{v}$. We can write the flux as a sum of the contributions from two distinct physical processes:

$$\mathbf{j} = \rho\mathbf{v} = \mathbf{j}_{\mathrm{dif}} + \mathbf{j}_{\mathrm{adv}}, \tag{2}$$

where $\mathbf{j}_{\mathrm{dif}}$ and $\mathbf{j}_{\mathrm{adv}}$ are diffusion and advection flux densities, respectively.

The diffusion flux is measured with respect to a frame of reference that is fixed to the crystal lattice. According to the Cahn–Hilliard nonlinear diffusion equation [21,22], the diffusion flux density is proportional to the gradient of chemical potential:

$$\mathbf{j}_{\mathrm{dif}} = -D\nabla\frac{\delta F}{\delta \rho}, \tag{3}$$

where $D(\mathbf{r})$ is the diffusion coefficient, and F is the system total free energy.

The total free energy F of a powder compact is a functional of the mass density field and structural order parameter fields. To describe the sintering process of a powder compact, we need to specify the shape, size, relative location, and crystallographic orientation of individual particles at every time moment, i.e., the powder compact microstructure and its evolution. In the phase field formalism, the microstructure evolution is conveniently described by the mass density field $\rho(\mathbf{r},t)$ in combination with a multicomponent structural order parameter field $\eta(\mathbf{r},t;\alpha = 1,2,\ldots,p)$, where the number of the order parameters, p, is equal to the number of particles in the powder compact. As shown schematically in Fig. 1, the mass density field $\rho(\mathbf{r},t)$ describes the distribution of solid material (or pores). The order parameters $\eta(\mathbf{r},t;\alpha)$ describe the geometry and crystallographic orientation of individual particles/grains, as in the phase field model of grain growth [14–16].

According to gradient thermodynamics [21], the total free energy F can be written in the following form:

$$F = \int_V \left[f(\rho, \{\eta(\alpha)\}) + \frac{1}{2}\beta_\rho |\nabla\rho|^2 + \sum_\alpha \frac{1}{2}\beta_\eta |\nabla\eta(\alpha)|^2 \right] \mathrm{d}^3 r, \tag{4}$$

where β_ρ and β_η are gradient coefficients. The function $f(\rho,\{\eta(\alpha)\})$ is the nonequilibrium bulk chemical free energy density that defines the homogeneous coexisting phases (solid and pore) and multiple solid domains (particles/grains of different crystallographic orientations). The second and third terms describe the energy contributions from surfaces and grain boundaries, respectively.

The local bulk chemical free energy function can be approximated by a Landau-type polynomial potential [31,32]. A particular form of this polynomial is:

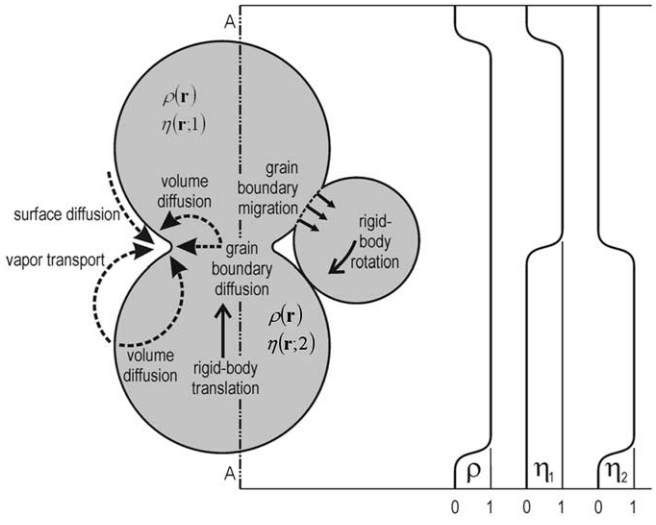

Fig. 1. Schematic of the phase field description of a powder compact using the mass density field $\rho(\mathbf{r})$ and order parameters $\eta(\mathbf{r};\alpha)$. The profiles of the field variables along the specified cross-section A–A cutting through two grains are plotted. Multiple concurrent physical processes treated by the proposed phase field sintering model are illustrated, including surface diffusion, grain boundary diffusion, volume diffusion, vapor transport, grain boundary migration, particle rigid-body translation and rotation.

$$f(\rho,\{\eta(\alpha)\}) = A\rho^2(1-\rho)^2 + B\left[\rho^2 + 6(1-\rho)\sum_\alpha \eta^2(\alpha) - 4(2-\rho)\sum_\alpha \eta^3(\alpha) + 3\left(\sum_\alpha \eta^2(\alpha)\right)^2\right], \quad (5)$$

where A and B are constants. The Landau-type potential of Eq. (5) is so constructed that the equilibrium value of mass density is reached at $\rho = 0$ in pores and $\rho = 1$ in solid particles, i.e., ρ being fractional mass density. The equilibrium value of the multicomponent order parameter vanishes in pores, i.e., $\{\eta(\alpha)\}_{\rho=0} = \{0,0,\ldots,0\}$, and is reached in solid at $\{\eta(\alpha)\}_{\rho=1} = \{1,0,\ldots,0\} = \ldots = \{0,0,\ldots,1\}$, which defines particles/grains of different crystallographic orientations. Thus, the local bulk chemical free energy "condenses" the spatial mass distribution into two phases: pores and solid particles/grains of different crystallographic orientations. The surface and grain boundary energies are characterized by the two gradient terms in Eq. (4) together with the local bulk chemical free energy over the diffuse interface regions of the field functions. It is noted that the polynomial form in Eq. (5) is different from that used in the two-phase grain growth model [30] in that it removes the unwanted even symmetry in the order parameter η and, thus, excludes the artificial grain boundaries between $\eta = -1$ and 1.

The various diffusion paths involved in sintering are characterized by the microstructural feature dependence of the diffusion coefficient in Eq. (3). In particular, the diffusion coefficient $D(\mathbf{r})$ is a function of the phase fields $\rho(\mathbf{r},t)$ and $\eta(\mathbf{r},t;\alpha)$:

$$D = D_{\mathrm{vol}}\phi(\rho) + D_{\mathrm{vap}}[1-\phi(\rho)] + D_{\mathrm{surf}}\rho(1-\rho) + D_{\mathrm{gb}}\sum_\alpha\sum_{\alpha'\neq\alpha}\eta(\alpha)\eta(\alpha'), \quad (6)$$

where $\phi = \rho^3(10 - 15\rho + 6\rho^2)$, and D_{vol}, D_{vap}, D_{surf} and D_{gb} are related to the diffusivity in solid bulk, vapor, along surface, and grain boundary, respectively. Using Eq. (6) with Eq. (3) automatically accounts for different diffusion mechanisms without explicitly tracking the surfaces or grain boundaries.

The advection flux describes the mass transport through a motion of a local volume element as a rigid body. In terms of advection velocity field $\mathbf{v}_{\mathrm{adv}}(\mathbf{r},t)$, we write the advection flux density as

$$\mathbf{j}_{\mathrm{adv}} = \rho\mathbf{v}_{\mathrm{adv}}. \quad (7)$$

In a sintering process, the advection velocity field is particularly simple. In addition to particle shape change by diffusion, each particle moves as a rigid body. The rigid-body motion consists of translation and rotation. The advection velocity field is a sum of the two contributions from all particles in the powder compact:

$$\mathbf{v}_{\mathrm{adv}} = \sum_\alpha \mathbf{v}_{\mathrm{adv}}(\alpha) = \sum_\alpha [\mathbf{v}_t(\alpha) + \mathbf{v}_r(\alpha)], \quad (8)$$

where $\mathbf{v}_t(\mathbf{r},t;\alpha)$ and $\mathbf{v}_r(\mathbf{r},t;\alpha)$ are the velocity fields associated with the translation and rotation of the αth particle, respectively.

The driving force for particle rigid-body motion arises from the role of grain boundaries as atom sources (or vacancy sinks), i.e., atoms diffuse away from grain boundaries to the nearby growing neck surfaces [1,9]. The chemical potential of atoms is lower at high-negative-curvature neck surfaces than at grain boundaries, and the grain boundary is a high-diffusivity path. Equivalently, vacancies flow from nearby neck surfaces into grain boundaries. The over-saturated vacancies are annihilated by the dislocations at grain boundaries, producing an effective local force that pulls neighboring particles toward one another through rigid-body translation and rotation. The approach of centers of particles through rigid-body motions plays a key role in the densification of sintered powder compacts [1,9]. If the particle rigid-body motions were absent, the over-saturation of vacancies would result in a mass density drop at grain boundaries. Computer simulation has demonstrated this effect [27]. In the phase field formalism, the effective local force density acting on the grain boundary of the αth particle can be formulated as:

$$\mathrm{d}\mathbf{F}(\alpha) = \kappa\sum_{\alpha'\neq\alpha}(\rho-\rho_0)\langle\eta(\alpha)\eta(\alpha')\rangle[\nabla\eta(\alpha) - \nabla\eta(\alpha')]\,\mathrm{d}^3r, \quad (9)$$

where κ is a stiffness constant relating the force magnitude to the vacancy over-saturation at grain boundaries (i.e., mass density variation with respect to its equilibrium value at grain boundaries). The constant ρ_0 characterizes the equilibrium value of mass density at grain boundaries, i.e., the force vanishes if $\rho = \rho_0$ at grain boundaries. The operation $\langle\eta(\alpha)\eta(\alpha')\rangle$ is defined as

$$\langle\eta(\alpha)\eta(\alpha')\rangle = \begin{cases} 1, & \text{if } \eta(\alpha)\eta(\alpha') \geqslant c, \\ 0, & \text{otherwise}, \end{cases} \quad (10)$$

where c is a threshold value in identifying grain boundaries through the order parameter product $\eta(\mathbf{r},\alpha)\eta(\mathbf{r},\alpha')$. It is noted that the gradient factor, $\nabla\eta(\alpha) - \nabla\eta(\alpha')$, in the local force equation is important for ensuring an action–reaction law between any pair of neighboring particles. A preliminary formula relating the effective force at grain boundaries to mass density change at grain boundaries was previously proposed [28] but was not further exploited to develop a working scheme for the phase field approach.

The resultant force and torque acting on the αth particle about its center of mass are

$$\mathbf{F}(\alpha) = \int_V \mathrm{d}\mathbf{F}(\alpha), \quad (11)$$

$$\mathbf{T}(\alpha) = \int_V [\mathbf{r} - \mathbf{r}_{\mathrm{c}}(\alpha)] \times \mathrm{d}\mathbf{F}(\alpha), \quad (12)$$

where the center of mass of the αth particle is

$$\mathbf{r}_{\mathrm{c}}(\alpha) = \frac{1}{V(\alpha)}\int_V \mathbf{r}\eta(\mathbf{r},\alpha)\,\mathrm{d}^3r, \quad (13)$$

and where the volume of the αth particle is

$$V(\alpha) = \int_V \eta(\mathbf{r}, \alpha)\, \mathrm{d}^3 r. \tag{14}$$

The velocity fields of rigid-body translation and rotation of the αth particle are

$$\mathbf{v}_\mathrm{t}(\mathbf{r}, \alpha) = \frac{m_\mathrm{t}}{V(\alpha)} \mathbf{F}(\alpha)\eta(\mathbf{r}, \alpha), \tag{15}$$

$$\mathbf{v}_\mathrm{r}(\mathbf{r}, \alpha) = \frac{m_\mathrm{r}}{V(\alpha)} \mathbf{T}(\alpha) \times [\mathbf{r} - \mathbf{r}_\mathrm{c}(\alpha)]\eta(\mathbf{r}, \alpha), \tag{16}$$

where m_t and m_r are constants characterizing the particle translation and rotation mobilities, respectively. An equation relating force to velocity instead of acceleration of rigid-body motion is employed because the rigid-body movement of particles in a powder compact is a highly dissipative process involving grain boundary sliding. The effects of sliding friction on particle movement can be taken into account by introducing force and torque threshold values into Eqs. (15) and (16) in calculating translation and rotation velocities, respectively.

The advection velocity field $\mathbf{v}_\mathrm{adv}(\mathbf{r}, t)$ over the whole powder compact is obtained by substituting Eqs. (15) and (16) into Eq. (8). Using the diffusion flux density (Eq. (3)) and advection flux density (Eq. (7)) with the equation of continuity (Eq. (1)) yields

$$\frac{\partial \rho}{\partial t} = \nabla \cdot \left(D \nabla \frac{\delta F}{\delta \rho} - \rho \mathbf{v}_\mathrm{adv} \right) + \xi_\rho(\mathbf{r}, t), \tag{17}$$

which is a nonlinear diffusion–advection equation. The Gaussian-distributed Langevin noise term $\xi_\rho(\mathbf{r}, t)$ accounts for the effect of thermal fluctuation and makes Eq. (17) stochastic [31]. It is noted that the introduction of rigid-body motions into the phase field model modifies the conventional Cahn–Hilliard equation [21,22] with an advection term.

Grain boundary migration is characterized by the time-dependent Ginzburg–Landau [23] (Allen–Cahn [24]) structural relaxation equation for the nonconserved multicomponent order parameter $\eta(\mathbf{r},t;\alpha)$, as in the phase field model of grain growth [14–16]. As in the case of diffusion, the presence of particle rigid-body motions also modifies the structural relaxation equation with an advection term:

$$\frac{\partial \eta(\alpha)}{\partial t} = -L \frac{\delta F}{\delta \eta(\alpha)} - \nabla \cdot [\eta(\alpha)\mathbf{v}_\mathrm{adv}(\alpha)] + \xi_\eta(\mathbf{r}, t; \alpha), \tag{18}$$

where L is a constant characterizing the mobility of grain boundary migration, and $\xi_\eta(\mathbf{r}, t; \alpha)$ is thermal noise.

The solutions $\rho(\mathbf{r}, t)$ and $\eta(\mathbf{r}, t; \alpha)$ to the kinetic Eqs. (17) and (18) provide the temporal and spatial evolutions of the field functions, which describe the microstructure evolution in powder compacts during sintering. The driving force for the evolution is a reduction in the system total free energy through multiple mass transport mechanisms and structural relaxation, i.e., reduction in surface energy and grain boundary energy through surface diffusion, grain boundary diffusion, volume diffusion, vapor transport, particle rigid-body motion, and grain boundary migration. The initial conditions $\rho(\mathbf{r}, t_0)$ and $\eta(\mathbf{r}, t_0;\alpha)$ describe the initial green compact microstructure, which could be an arbitrary nonequilibrium state or a predefined state of interest. In computer simulations, the microstructure evolves to reduce the total free energy by automatically following a favorable kinetic pathway, without an a priori constraint imposed on the evolution path.

3. Simulation

In computer simulations, the phase field equations are discretized with respect to space and time by using the finite difference and explicit forward Euler scheme. The equations are also nondimensionalized with respect to the computational grid size l_0 and the energy barrier Δf between the two coexisting phases (solid and vapor). The values of the reduced parameters used in the simulations are: $\beta^*_\rho = 10$ and $\beta^*_\eta = 1$ in Eq. (4), $A^* = 16$ and $B^* = 1$ in Eq. (5), $D^*_\mathrm{vol} = 0.01$, $D^*_\mathrm{vap} = 0.001$, $D^*_\mathrm{surf} = 4$, and $D^*_\mathrm{gb} = 0.4$ in Eq. (6), $\kappa = 100$ and $\rho_0 = 0.9816$ in Eq. (9), $c = 0.14$ in Eq. (10), $m_t = 500$ in Eq. (15), $m_r = 1$ in Eq. (16), $L^* = 10$ in Eq. (18), ans $\xi^*_\rho = 0$, and $\xi^*_\eta = 0$ in Eqs. (17) and (18), respectively. These parameters give a diffusivity ratio of about 1000:100:10:1 along surface and grain boundary, through volume and vapor, respectively, and an interfacial energy density ratio of about 2:1 between surface and grain boundary. These values could also be taken from physical quantities related to specific materials. The developed phase field sintering model is formulated for the general cases of 3D powder compacts. Two-dimensional (2D) simulations are performed in the following for demonstration.

Simulations are performed to study the particle shape change through different mass transport modes, i.e., through volume and vapor, along surface and grain boundary, and with all mass transport modes active. Fig. 2 shows

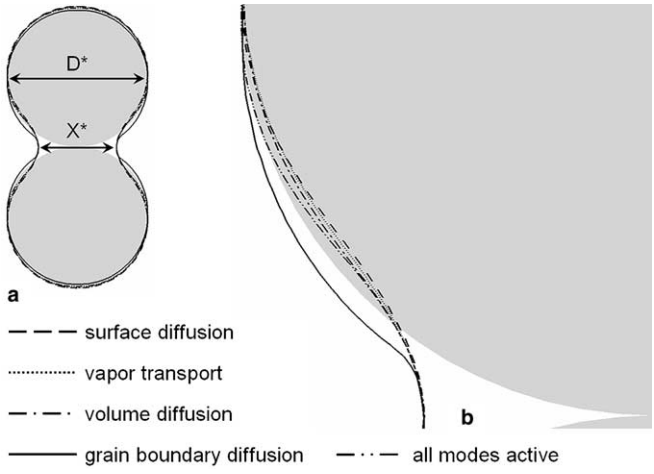

Fig. 2. Simulated neck growth and particle shape change during sintering through different mass transport modes, i.e., through volume or vapor, along surface or grain boundary, or with all mass transport modes active. (a) The comparison of particle shape changes through different mass transport modes indicated by different line patterns is made at the same stage of neck growth with $X^* = 44$ and $D^* = 80$, where the gray shadow shows the initial shape. (b) A close-up view of a portion of (a).

the particle shape changes. To make the comparison clearer, the same stage of neck growth is considered, i.e., at neck size $X^* = 44$ with particle size $D^* = 80$, as shown in Fig. 2(a). It is evident from the close-up view shown in Fig. 2(b) that only grain boundary diffusion with the resultant rigid-body motions leads to approach of the particle centers (i.e., shrinkage). Other mass transport modes only change particle shape but do not contribute to powder compact shrinkage. Instead, they compete with grain boundary diffusion during neck growth and reduce the amount of shrinkage, as shown by the simulation with all mass transport modes active.

A detailed analysis is performed to study the laws of neck growth and shrinkage by fitting the simulation results to a power law. Simplified sintering models for initial-stage neck growth provide an estimate of the rate of change of neck size ratio as a function of sintering time, which has a representative form, $(X/D)^n = Kt$ [1], where K is a term related to material properties and geometrical assumptions. To compare the phase field simulations with such models, it is noted that while the phase field model asymptotically approaches the sharp interface model in the limit of vanishing interface thickness [17] and it is accurate when microstructure feature size is much larger than the thickness of diffuse interfaces, the very initial stage of neck growth is a situation involving large surface curvature and, thus, the phase field simulation may produce certain artifacts. To reduce the effect of artifacts on the growth law, an initial time t_0 is introduced to the exponential function, which is to be determined as an extra fitting parameter. By fitting simulated neck growth under different mass transport mechanisms to the function $(X^*/D^*)^n = K^*(t^* - t_0^*)$, the fitting parameters n, K^*, and t_0^* are obtained. The exponent n has particular significance since it reflects the dominant sintering mechanism. The values of n for different simulated sintering mechanisms are summarized in Table 1, where also shown are predictions from analytical models [1] for comparison. It is noted that such a comparison is not always appropriate, since analytical models are applicable to the initial stage of neck growth ($X/D < 0.3$) under simplifying geometrical assumptions. Although analytical models are generally derived for neck growth of two equal spheres (i.e., 3D model) by a single mass transport mechanism, the exponent n usually remains the same in the 2D case. However, depending on different assumptions, different models predict widely different n for the same mass transport mechanism, e.g., n values of 3, 5, 6, 7, and 7.5 have been predicted for surface diffusion [1]. The value of n also changes with the degree of sintering (sintering time and neck size). To illustrate this change, the n values are determined by fitting the results of different simulation times, i.e., for $t^* < 20$ and $t^* < 100$, and are listed in Table 1. While the change in n value is relatively small in all other mass transport modes, n increases significantly from 5.52 to 9.04 in grain boundary diffusion, indicating significant slowing down in the neck growth rate through grain boundary diffusion. This could be attributed to longer diffusion path along the grain boundary to the neck surface and, thus, slower diffusion kinetics. The simulated neck growth through grain boundary diffusion and the fitted growth law curves for different simulation times are shown in Fig. 3(a).

Similarly, a power law of shrinkage is also fitted to find the exponent n', i.e., $(\Delta L^*/L_0^*)^{n'} = M^*(t^* - t_0^*)$, where ΔL^* is the length change (approaching distance of particle centers), and $L_0^* = 2D^*$ is the initial reference length. We obtain $n' = 3.16$ for $t^* < 20$ and $n' = 5.12$ for $t^* < 100$ in grain boundary diffusion, which is the only mechanism leading to shrinkage. According to Ref. [1], a simple relation $n'/n = 0.5$ holds. The simulations give $n'/n = 0.572$ for $t^* < 20$ and $n'/n = 0.566$ for $t^* < 100$. The simulated shrinkage and the fitted power law curves are shown in Fig. 3(b). It shows that the earlier stage of neck growth is most important for shrinkage and densification.

The parameters used in the simulations give an interfacial energy density ratio of about 2:1 between surface and grain boundary. As a result, a dihedral angle of $\phi \approx 150°$ should form at the neck surface. Such a dihedral angle is not evident in Fig. 2, where the particles are visualized through the mass density field $\rho(\mathbf{r})$. We can also visualize the particles through the structural order parameter fields $\eta(\mathbf{r};\alpha)$, as shown in Fig. 3(c), which clearly shows the formation of a dihedral angle $\phi \approx 150°$ at the neck surface. The reason for this different visualization effect is that the surface energy is characterized by the gradient terms of $\rho(\mathbf{r})$ and $\eta(\mathbf{r};\alpha)$ together, while the grain boundary energy is characterized mainly by $\eta(\mathbf{r};\alpha)$ alone, as formulated in Eq. (4) and illustrated in Fig. 1. The two types of fields $\rho(\mathbf{r})$ and $\eta(\mathbf{r};\alpha)$ are coupled through Eq. (5), while the coupling between their gradient terms is indirect. This gives a small artifact in the field $\rho(\mathbf{r})$ at the junction of surface and grain boundary where surface curvature is large. However, it is noted that the energetics of surfaces and grain boundaries is correct in the phase field simulation, and the error associated with this minor artifact is small, as demonstrated by the formation of the correct dihedral angle shown in Fig. 3(c). It is further noted that the small angle formed at the beak-like neck groove is again associated with the diffuse interface effect of the structural order parameter fields $\eta(\mathbf{r};\alpha)$.

Fig. 4 shows the simulated microstructure evolution in a 2D sintered powder compact consisting of 26 particles [37]. The particle number, size distribution, and spatial arrangement in the initial green compact are prepared arbitrarily in this simulation, as shown in Fig. 4(a). Figs. 4(b)–(d) show three typical snapshots of the simulated sintering process. The removal of pores is highlighted by dotted lines. Grain boundary migration is evident. The simulation shows that the removal of bigger pores has very slow kinetics, which was not reached within our simulation time.

4. Discussion

In this paper, a phase field model of solid-state sintering is developed. We start with the equation of continuity and

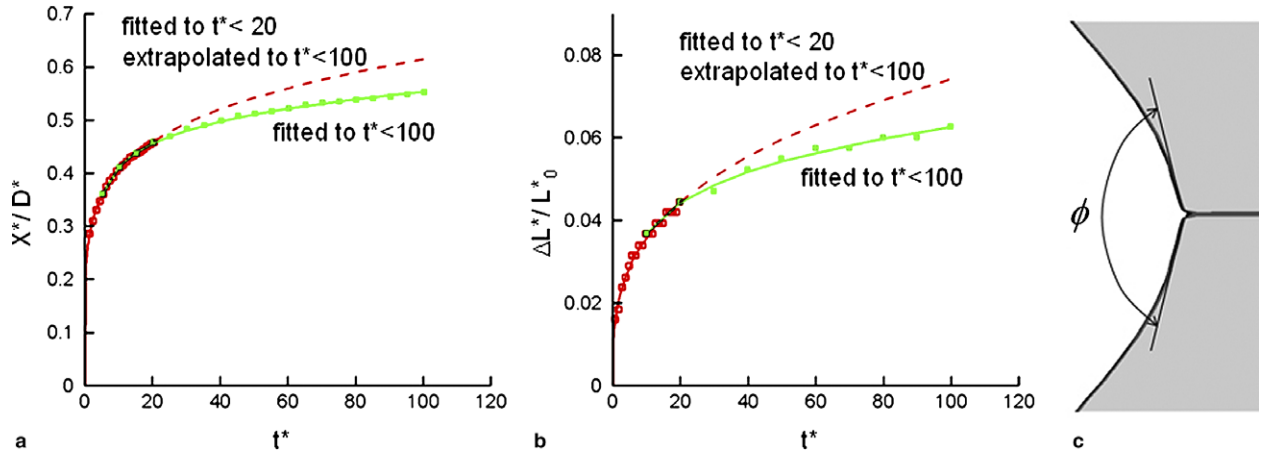

Fig. 3. Simulated neck growth (a) and shrinkage (b) in grain boundary diffusion. The curves are fitted to power laws for different simulation times. (c) Structural order parameter visualization of the simulated neck growth and particle shape change during sintering with all mass transport modes active. A groove with dihedral angle is formed at the neck surface.

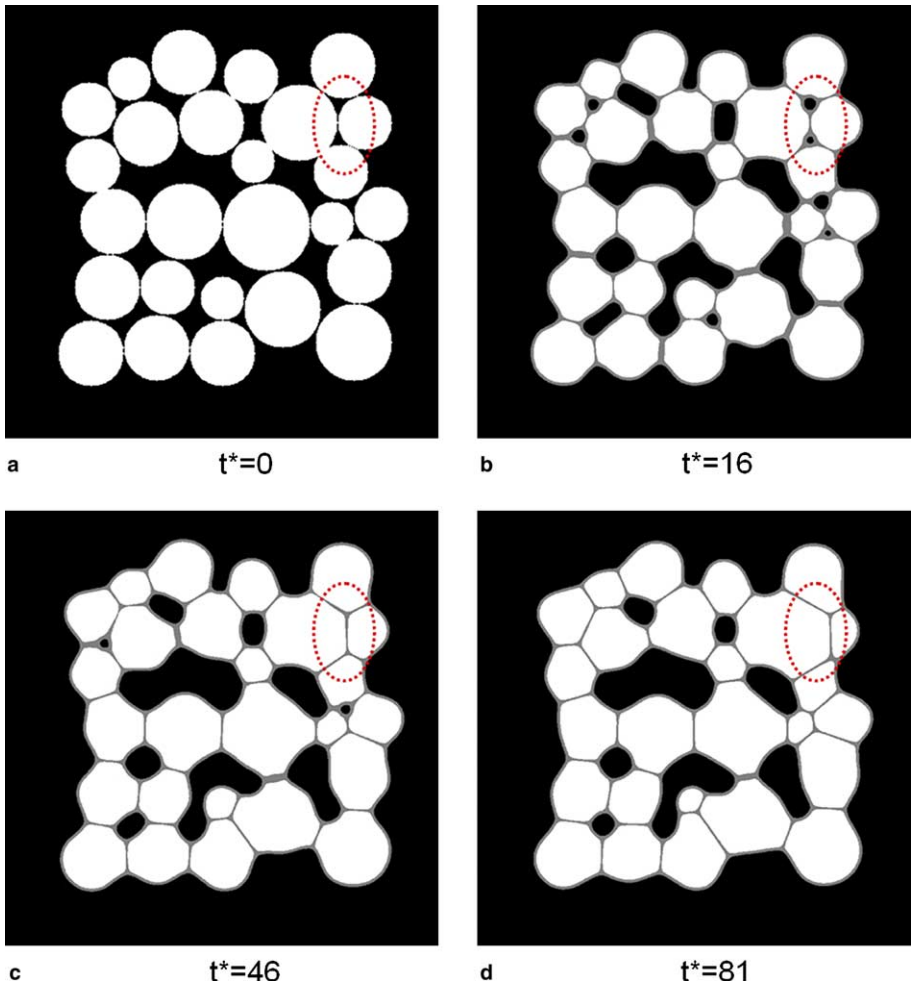

Fig. 4. Simulated microstructure evolution in a powder compact during sintering [37]. (a) Initial green compact. (b–d) Typical snapshots of the simulated sintering process shown in reduced simulation time. One area is highlighted by dotted lines to show the removal of two pores and subsequent grain boundary migration.

separate the mass flux into two distinct contributions from diffusion and rigid-body motion. The diffusion is characterized by the Cahn–Hilliard nonlinear diffusion equation [21,22]. The various diffusion paths involved in sintering (along surface and grain boundary, through bulk lattice and vapor) are automatically characterized by the dependence

of the diffusion coefficient on the microstructural features of the powder compact through the phase field variables without explicitly tracking the surfaces or grain boundaries, as formulated in Eq. (6). The grain boundary migration is characterized by the time-dependent Ginzburg–Landau [23] (Allen–Cahn [24]) structural relaxation equation, as in the phase field model of grain growth [14–16]. The advection mass flux associated with the particle rigid-body motions is an essential component of the proposed phase field sintering model. The driving force for particle rigid-body translation and rotation results from the role of grain boundaries as vacancy sinks [1,9], which produces effective forces acting at grain boundaries and pulling neighboring particles towards one another. The rigid-body motion modifies both Cahn–Hilliard and Ginzburg–Landau (Allen–Cahn) equations by introducing advection terms, which become nonlinear diffusion–advection and structural relaxation–advection equations, respectively.

The main obstacle to developing a phase field sintering model is associated with the difficulty in treating the particle rigid-body motions in an effective way consistent with phase field formalism, i.e., without explicitly imposing boundary conditions at grain boundaries. A preliminary formula relating the effective force at grain boundaries to mass density change at grain boundaries was previously reported [28], but was not further developed into a working scheme for the phase field approach. Instead, a boundary condition of mass conservation was explicitly imposed at grain boundaries and only simulation of planar grain boundaries at fixed spatial position has been reported [27,28]. It is noted that an explicit treatment of grain boundary conditions prevents the effective application to the phase field simulation of realistic sintering processes involving complicated powder compact microstructures. In this paper, we propose the local force formula, Eq. (9), and formulate the advection velocity field associated with particle rigid-body translation and rotation, Eqs. (11)–(16). Eq. (9) introduces a mathematical device, whose role is, in effect, to connect neighboring grains with a layer of elastic "glue", which tries to maintain an equilibrium mass density at grain boundaries. The neighboring particles are pulled closer or pushed further apart according to the mass density variation at their mutual grain boundary. The local force density $d\mathbf{F}(\alpha)$ in Eq. (9) is formulated in terms of the phase field functions $\rho(\mathbf{r},t)$ and $\eta(\mathbf{r},t;\alpha)$ without explicitly tracking grain boundaries, which is consistent with the phase field formalism. Eq. (9) has two important features. The first feature is an operation $\nabla\eta(\alpha)-\nabla\eta(\alpha')$ to ensure an action–reaction law between any pair of neighboring particles indexed by α and α'. Because of the discretization of the continuous phase field equations into computational grids, both the magnitude and direction of the forces calculated for two neighboring grains could be different when evaluated at discrete computational grids. Such an artifact is removed by the operation $\nabla\eta(\alpha)-\nabla\eta(\alpha')$. The second feature is a threshold operation $\langle\eta(\alpha)\eta(\alpha')\rangle$ defined in Eq. (10) to identify correctly grain boundaries through diffuse interface field functions and exclude the region around the neck surface where $\eta(\mathbf{r},\alpha)\eta(\mathbf{r},\alpha')$ does not completely vanish while $\rho(\mathbf{r})$ significantly drops below the equilibrium value ρ_0. The force–velocity formulae of Eqs. (15) and (16) assume an inverse proportionality to the particle volume, which ensures a law of inertia for the whole powder compact during free sintering, i.e., the center of mass of the powder compact does not change. In the case of constrained sintering, e.g., powder sintered on a substrate surface, the forces from the substrate acting on the particles in contact with the substrate will produce a net displacement of the whole powder compact. It is noted that in computer simulation, when one grain shrinks to disappear, a vanishing volume could result in numerical problems in evaluating Eqs. (15) and (16). In such a case, a small but finite value should be used instead of the true volume. The artifact associated with this procedure is negligible.

The Landau-type polynomial potential in Eq. (5) proposed in this paper is different from that used in the phase field model of grain growth [14–16,30]. It removes the unwanted even symmetry in the order parameter η, thus automatically excluding the artificial grain boundaries between $\eta=-1$ and 1. It is noted that if the particle rigid-body motion is switched off, i.e., $m_t=m_r=0$ in Eqs. (15) and (16), the proposed phase field model of solid-state sintering is reduced to the phase field model of two-phase grain growth [30] with a different form of Landau-type polynomial potential. In such a case, one of the coexisting phases is crystalline grains, while the second phase is amorphous (vapor or pore). The structural order parameters are used to characterize the grains of different crystallographic orientations, while no order parameter is needed for the amorphous phase.

In the simulations presented in this paper, an explicit forward Euler finite difference scheme is used. More advanced algorithms can be used. In particular, the semi-implicit Fourier-spectral method has been shown to be orders of magnitude more efficient [33,34].

Isotropic grain boundary energy is assumed in this paper. Anisotropic grain boundary energy (and also mobility) can be treated in the same manner as in the phase field model of grain growth in anisotropic systems [16]. To do this, we need to introduce a simple bookkeeping scheme to record the specific Euler angles that uniquely define the crystallographic orientation of individual grains. The Euler angles are updated by the particle rigid-body rotation determined in Eq. (16) and give the misorientations between neighboring grains, which are then used to calculate grain boundary energies. Such an approach to anisotropic grain boundary energy has been developed for 2D grain growth simulations [16].

Considering stress effects on sintering kinetics in the proposed phase field sintering model is straightforward. A phase field microelasticity theory of 3D elastically anisotropic solids with arbitrary elastic modulus mismatch and crystal lattice misfit has been developed [35,36]. Incorporating this

theory into the sintering model will allow us to simulate stress-assisted sintering processes, such as hot isostatic pressing and uniaxial and triaxial hot pressing. Based on the phase field models of solid-state phase transformations (e.g., summarized in Ref. [11]), phase transformations can also be incorporated into the proposed phase field sintering model.

A phase field model of multiple phase sintering can also be developed. The main difference is in the Landau-type polynomial. To characterize multiple phases, each solid phase requires a mass density field and a multiple-component structural order parameter. In the case of no chemical reaction among phases, the multiple-phase sintering model is similar to the sintering model developed in this paper and will be reported elsewhere.

Acknowledgements

The author is grateful to the valuable discussion with Dr. Armen G. Khachaturyan (Ceramic & Materials Engineering, Rutgers University) and Dr. Yongmei M. Jin (Aerospace Engineering, Texas A&M University). The computer simulation was performed on NPACI Data Star at San Diego Supercomputer Center and System X at Virginia Tech. The financial support from Virginia Tech through a startup fund is acknowledged.

References

[1] German RM. Sintering theory and practice. New York (NY): John Wiley; 1996.
[2] Patankar KK, Dombale PD, Mathe VL, Patil SA, Patil RN. Mater Sci Eng B 2001;87:53.
[3] Ryu J, Carazo AV, Uchino K, Kim HE. J Electroceram 2001;7:17.
[4] Zhai JY, Cai N, Liu L, Lin YH, Nan CW. Mater Sci Eng B 2003;99:329.
[5] Zhai J, Cai N, Shi Z, Lin Y, Nan CW. J Phys D 2004;37:823.
[6] Seal S, Baraton MI. MRS Bull 2004;29:9.
[7] Choe JW, Calata JN, Lu GQ. J Mater Res 1995;10:986.
[8] Calata JN, Lu GQ, Chuang TJ. Surf Interf Anal 2001;31:673.
[9] Kingery WD, Bowen HK, Uhlmann DR. Introduction to ceramics. 2nd ed. New York (NY): John Wiley; 1976.
[10] Olevsky EA. Mater Sci Eng R 1998;23:41.
[11] Chen LQ. Annu Rev Mater Res 2002;32:113.
[12] Boettinger WJ, Warren JA, Beckermann C, Karma A. Annu Rev Mater Res 2002;32:163.
[13] Wang Y, Chen LQ. In: Methods in material research, a current protocols publication. New York (NY): John Wiley; 2000. p. 2a.3.1.
[14] Chen LQ, Yang W. Phys Rev B 1994;50:15752.
[15] Krill III CE, Chen LQ. Acta Mater 2002;50:3057.
[16] Kazaryan A, Wang Y, Dregia SA, Patton BR. Acta Mater 2002;50:2491.
[17] Elder KR, Grant M, Provatas N, Kosterlitz JM. Phys Rev E 2001;64:021604.
[18] Khachaturyan AG. Theory of structural transformation in solids. New York (NY): John Wiley; 1983.
[19] Li YL, Hu SY, Liu ZK, Chen LQ. Acta Mater 2002;50:395.
[20] Jin YM, Wang YU, Kazaryan A, Wang Y, Laughlin DE, Khachaturyan AG. J Appl Phys 2002;92:6172.
[21] Cahn JW, Hilliard JE. J Chem Phys 1958;28:258.
[22] Cahn JW. Acta Metall 1961;9:795.
[23] Ginzburg VL, Landau LD. Sov Phys JETP 1950;20:1064.
[24] Allen SM, Cahn JW. Acta Metall 1979;27:1085.
[25] Hohenberg PC, Halperin BI. Rev Mod Phys 1977;49:435.
[26] Gunton JD, Miguel MS, Sahni PS. In: Domb C, Lebowitz JL, editors. Phase transitions and critical phenomena. New York (NY): Academic Press; 1983. p. 267.
[27] Kazaryan A, Wang Y, Patton BR. Scripta Mater 1999;41:487.
[28] Kazaryan A, Shen C, Wang Y, Patton BR. In: Turchi PEA, Gonis A, editors. Phase transformations and evolution in materials. Warrendale (PA): TMS; 2000. p. 89.
[29] Wang Y, Chen LQ, Khachaturyan AG. Phys Rev B 1992;46:11194.
[30] Fan D, Chen LQ. Scripta Mater 1997;37:233.
[31] Landau LD, Lifshitz EM. Statistical physics. 3rd ed. Oxford: Pergamon Press; 1980.
[32] Toledano P, Dmitriev V. Reconstructive phase transitions in crystals and quasicrystals. Singapore: World Scientific; 1996.
[33] Chen LQ, Shen J. Comput Phys Commun 1998;108:147.
[34] Zhu J, Chen LQ, Shen J, Tikare V. Phys Rev E 1999;60:3564.
[35] Wang YU, Jin YM, Khachaturyan AG. Appl Phys Lett 2002;80:4513.
[36] Wang YU, Jin YM, Khachaturyan AG. J Appl Phys 2002;92:1351.
[37] Wang Y. (unpublished).